Spin and orbital ordering in Y_{1−x}La_{x}VO_{3}

J.-Q. Yan, J.-S. Zhou, J. G. Cheng, J. B. Goodenough, Y. Ren, A. Llobet, and R. J. McQueeney

Phys. Rev. B **84**, 214405 — Published 2 December 2011

DOI: 10.1103/PhysRevB.84.214405

Spin and orbital ordering in $Y_{1-x}La_xVO_3$

J.-Q. Yan,[1*] J.-S. Zhou,[2] J.G. Cheng,[2] J. B. Goodenough,[2] Y. Ren,[3] A. Llobet,[4] and R. J. McQueeney[1,5]

[1]Ames Laboratory, US-DOE, Ames, IA 50011

[2]Texas Materials Institute, the University of Texas at Austin, Austin, TX 78712

[3]X-ray Diffraction Division, Argonne National Laboratory, Argonne, IL 60439

[4] Los Alamos Neutron Science Center, Lujan Neutron Scattering Center, Los Alamos National Laboratory, Los Alamos, NM 87545

[5]Department of Physics and Astronomy, Iowa State University, Ames, IA 50011

Abstract

The spin and orbital ordering in $Y_{1-x}La_xVO_3$ ($0.30 \leq x \leq 1.0$) has been studied to map out the phase diagram over the whole doping range $0 \leq x \leq 1$. The phase diagram is compared with that for RVO_3 (R = rare earth or Y) perovskites without A-site variance. For $x > 0.20$, no long-range orbital ordering was observed above the magnetic ordering temperature T_N; the magnetic order is accompanied by a lattice anomaly at a $T_t \leq T_N$ as in $LaVO_3$. The magnetic ordering below $T_t \leq T_N$ is G-type in the compositional range $0.20 \leq x \leq 0.40$ and C-type in the range $0.738 \leq x \leq 1.0$. Magnetization and neutron powder diffraction measurements point to the coexistence below T_N of the two magnetic phases in the compositional range $0.4 < x < 0.738$. Samples in the compositional range $0.20 < x \leq 1.0$ are characterized by an additional suppression of a glass-like thermal conductivity in the temperature interval $T_N < T < T^*$ and a change in the slope of $1/\chi(T)$. We argue that

T* represents a temperature below which spin and orbital fluctuations couple together via $\lambda \mathbf{L} \bullet \mathbf{S}$.

PACS: 61.05.F-, 61.05.cp, 65.40.ba, 71.70.Ej, 75.30.Cr

Introduction

The orthorhombic (Pbnm) RVO_3 perovskites (R = rare earth or Y) are a single-valent family in which the octahedral-site V^{3+}:t^2e^0 ions have only π-bonding *t* electrons that are Jahn-Teller active. All RVO_3 members show multiple spin and orbital orderings[1, 2, 3, 4] as is shown in Fig 1(a), thus providing a unique opportunity to study the spin-orbital-lattice coupling of π-bonding *t* electrons. Among the RVO_3 members, $LaVO_3$ and YVO_3 are of particular interest since (1) the La^{3+} and Y^{3+} ions carry no moment either to obscure the magnetic behavior of the VO_3 array or to interact with it, and (2) $LaVO_3$ and YVO_3 have a different sequence of spin and orbital ordering. With decreasing temperature, YVO_3 undergoes a second-order transition to G-type orbital ordering (G-OO) at T_{OO} = 200 K, a second-order transition to C-type antiferromagnetic order (C-SO) at T_N = 116 K, and a first-order orbital flipping transition at T_{CG} = 77 K. A C-type orbital order (C-OO) and a G-type antiferromagnetic order (G-SO) observed below T_{CG} are in contrast to G-OO/C-SO seen in the temperature interval $T_{CG} < T < T_N$. On cooling $LaVO_3$, on the other hand, an antiferromagnetic transition at T_N = 143 K is followed by a first-order transition at $T_t = T_N - 3.5$ K to a G-OO/C-SO phase that is stable to lowest

temperatures. In this 3.5 K interval, a C-OO/G-SO state has been suggested.[3,5] The system $Y_{1-x}La_xVO_3$ allows a study of the evolution of the several transition temperatures with average R^{3+}-ion radius without interference from a magnetic moment on the R^{3+} ion, but at the price of introducing variance σ^2 of the R^{3+}-ion radius:

$$\sigma^2 = \sum_i x_i r_i^2 - < r_i >^2$$

where x_i is the concentration of each R^{3+} ion of ionic radius r_i. [6] An earlier attempt[7] to synthesize this system by solid-state reaction failed due to phase separation in the interval $0.08 < x < 0.92$. With the aid of an image furnace, we have been able to synthesize single-phase $Y_{1-x}La_xVO_3$ over the entire compositional range $0 \leq x \leq 1$. The doping dependence of the orbital and spin ordering for $Y_{1-x}La_xVO_3$ in the composition interval $0 \leq x < 0.20$ has been well-studied and reported elsewhere. [8] In this range, the partial replacement of Y by La increases the average R^{3+}-ion radius (IR) and $(180°-\phi)$ V-O-V bond angle; both T_{OO} and T_N decrease while T_{CG} increases with x (see Fig 1 (b)). This IR dependence of the transition temperatures is opposite to that in Fig 1(a). A comparative study[8] of the physical properties of $Y_{1-x}(La_{0.23}Lu_{0.77})_xVO_3$, where the variation of x changes the A-site variance only while keeping the average A-site size constant, has unambiguously demonstrated that the A-site variance is playing a major role in determining the critical temperatures in La (and Lu) doped compositions. Thermal-conductivity and specific-heat data for $Y_{1-x}La_xVO_3$ $(0 \leq x < 0.20)$ showed that an R^{3+}-ion variance lowers the stability of G-OO/C-SO relative to that of C-OO/G-SO.

In order to explore the evolution of spin and orbital ordering with La-doping in the whole composition range, we have extended our study to compositions in the interval

$0.30 \leq x \leq 1.0$ by measuring magnetic properties, thermal conductivity, and specific heat. The corresponding magnetic and crystal-structure changes associated with the spin and orbital ordering were also studied by synchrotron x-ray and neutron powder diffraction. In this paper, we report the evolution of the spin/orbital ordering and present a phase diagram for all values of x.

Experiment

Single-phase $Y_{1-x}La_xVO_3$ ($0.30 \leq x \leq 1$) samples were melt-grown with the aid of an image furnace in a procedure described elsewhere, [9] but with special attention to prevent any composition segregation. All samples in the composition interval $0.30 \leq x < 1.0$ are well-crystallized polycrystals and were confirmed to be single-phase at room temperature by x-ray powder diffraction. The room-temperature patterns could be indexed in Pbnm symmetry. No superlattice peaks due to Y/La ordering were observed. The lattice parameters and unit-cell volume vary systematically with increasing La content (see Fig. 2). A large thermoelectric power (> 550 μV/K) at room temperature implies an essentially stoichiometric oxygen content. The magnetic properties were measured with a Magnetic Property Measurement System (Quantum Design, QD) in the temperature interval $5\ K \leq x \leq 300\ K$. Specific heat was measured with a Physical Properties Measurement System (QD) in the temperature interval $2\ K \leq T \leq 300\ K$. Thermal conductivity was measured with a home-made setup in the temperature interval $5\ K \leq T \leq 300\ K$. The high energy high resolution x-ray powder diffraction was performed at 11ID-C, Advanced Photon Source, Argonne National Laboratory. Neutron powder diffraction for x = 0.90 and 1.0 was performed at SEPD, Intense Pulsed Neutron

Source, Argonne National Laboratory, and for all other compositions at HIPD, Los Alamos Neutron Science Center, Los Alamos National Laboratory.

Results

The magnetic susceptibilities of compositions with $x \leq 0.30$ measured in a zero-field-cool (ZFC) mode at 1 kOe have been reported elsewhere.[8] In the composition interval $0 \leq x \leq 0.18$, T_{OO} and T_N decrease with increasing doping while T_{CG} increases until it intersects T_N at $x \approx 0.20$. The evolution of T_{OO}, T_N, and T_{CG} with doping for $x < 0.20$ has been further confirmed by specific-heat and thermal-conductivity data. These earlier results are included in the phase diagram of Fig 1(b). At $x = 0.20$, T_N suddenly increases and no other anomaly was observed below or above T_N, which signals the disappearance of T_{OO} and T_{CG}. For $x = 0.30$, the magnetic susceptibility shows a temperature dependence similar to that for $x = 0.20$, but with a higher T_N.

Figure 3(a) shows the temperature dependence of magnetic susceptibility of $Y_{1-x}La_xVO_3$ ($0.30 \leq x \leq 0.858$) measured in ZFC and FC modes at 1 kOe. Only one long-range magnetic/orbital ordering temperature T_N was observed. An obvious splitting between ZFC and FC curves below T_N can be seen. T_N, which is defined as the temperature where FC and ZFC curves split, increases with increasing La content in the intervals $0.20 \leq x \leq 0.40$ and $0.738 < x \leq 1$; it stays more or less constant in the interval $0.40 \leq x \leq 0.738$. In a study of the magnetic properties of $LaVO_3$, YVO_3 and $LuVO_3$, Yan *et al*[10] found that the orbital flipping transition at T_{CG} affects the splitting between FC and ZFC curves; FC and ZFC curves overlap if the measurement crosses the orbital

flipping transition at T_{CG}. Figure 3(b) shows the doping dependence of the splitting between FC and ZFC curves at 5 K. For $x \leq 0.18$, FC and ZFC curves overlap in the whole temperature range, which is consistent with the fact that the orbital flipping transition takes place at $T_{CG} < T_N$. Splitting of the FC and ZFC curves sets in at $x = 0.20$, which signals that orbital flipping at a T_{CG} disappears at $x = 0.20$. The splitting reaches a maximum at $x \approx 0.50$ and then decreases with a further increase of the La content; at $x = 0.858$, the FC curve is smaller in magnitude than the ZFC curve at low temperatures. This evolution of the splitting between the FC and ZFC curves signals the appearance of the G-OO/C-SO phase below T_N for $x > 0.50$, the volume fraction of this phase growing with x until it reaches unity in the interval $0.738 \leq x \leq 0.858$, since a weak magnetization opposite to the magnetizing field is found at low temperatures in the G-OO/C-SO phase.[7]

Figure 4(a) shows the temperature dependence of $1/\chi(T)$ of $Y_{1-x}La_xVO_3$ ($0.0 \leq x \leq 1.0$) above the magnetic ordering temperature. The orbital ordering at T_{OO} has been found to induce a slope change of the $1/\chi(T)$ curve.[11] As highlighted by solid arrows, a slope change could be observed for all the compositions with $x \leq 0.18$, which signals the orbital ordering to G-type takes place above T_N for all these compositions. T_{OO} is lowered with increasing La content. For $x = 0.20$, $1/\chi(T)$ is almost linear in the whole temperature range above T_N; a slope change at $T \approx 140$ K is barely observable. For $0.30 \leq x \leq 1.0$, a slope change could also be observed at 50 to 80 K above T_N, but the slope change is in an opposite direction compared to those in compositions with $x \leq 0.18$. Figure 4(b) shows the derivative of $\chi(T)$ for compositions around $x = 0.20$ to highlight the evolution of slope change with increasing La doping. We denote by T^* those temperatures where

$1/\chi(T)$ deviates from a linear temperature dependence for $x \geq 0.30$. Interestingly, a slope change in the T-dependence of thermal conductivity, $\kappa(T)$, was also observed at T^* for $x \geq 0.30$.

Figure 5 shows $1/\kappa(T)$ of x= 0.40, 0.738, and 0.858. The temperature dependence of $1/\kappa(T)$ is similar to that of $LaVO_3$ and $CeVO_3$ by showing a glass-like heat transport above T^* and an additional suppression of $\kappa(T)$ in the interval $T_N \leq T \leq T^*$. The measured samples are all well-crystallized, but polycrystalline. A large $1/\kappa(T)$ signals significant scattering from grain boundaries. The scattering broadens and weakens the transition at T_N, which makes it difficult to accurately determine T_N from the $\kappa(T)$ data. However, this scattering cannot be responsible for the glass-like thermal conductivity above T_N for well-crystallized samples. In the paramagnetic state of an insulating perovskite, phonons are the primary heat carrier. As discussed in Ref [9], the observed glassy phonon behavior at $T > T_N$ can only be explained by spin and orbital fluctuations. A slope change at T^* where $1/\kappa(T)$ deviates from a linear temperature dependence signals that the lattice heat transport is more strongly disturbed in the temperature interval $T_N \leq T \leq T^*$. This additional suppression at T* further confirms the absence of a long-range orbital ordering above T_N.

Figure 6 shows specific-heat data for x = 0.50 where only one magnetic/orbital ordering temperature has been determined from the magnetic measurement. As expected, only one lambda anomaly was observed. This is in contrast to the specific-heat data for $x \leq 0.16$ where three transition temperatures, T_{OO}, T_N, and T_{CG}, could be unambiguously

resolved from high-quality specific heat data.[8] In order to estimate the entropy release associated with orbital and/or spin ordering, the lattice contribution has to be estimated and subtracted from the total specific heat. For this purpose, we estimated the lattice specific heat with the Thirring model: [12,13]

$$C_{lattice} = 3NR(1 + \sum_{n=1}^{\infty} b_n \mu^{-n})$$

where N is the number of atoms in the unit cell, R is the ideal gas constant, $\mu = (2\pi T/\theta_D)^2+1$, and θ_D is the Debye temperature. This model can achieve an accuracy of ~ 0.03% with only four terms for a Debye solid at $T = \theta_D/4$. In our fitting, we use n = 4 and obtained a reasonable accuracy as demonstrated by the dashed curve in Fig 6. By subtracting the lattice specific heat, we obtained the entropy change involved in the transition from the area under the lambda anomaly in a C_p/T versus T plot.

In order to confirm the validity of our fitting, we calculated the entropy change around T_{OO} and T_N for YVO_3 and compared it with a previous report. For YVO_3, the obtained entropy changes associated with G-OO and C-SO orderings are 1.56 J/(mol K) and 0.61 J/(mol K), respectively. These values agree well with those reported by Blake *et al*.[14] La doping increases T_{CG} while lowering T_N in the composition interval $0 \leq x \leq 0.18$. The narrow temperature interval between T_N and T_{CG} makes it difficult to estimate the entropy change associated with magnetic order at T_N. Thus we calculated only the entropy change involved in the orbital ordering at T_{OO} for $x \leq 0.18$. Figure 7 shows the compositional dependence of the entropy change associated with G-type orbital order around T_{OO}. La doping reduces the entropy change on crossing T_{OO}, which implies that

the orbital degree of freedom is not totally quenched below T_{OO}. If we define T_{OO} as the temperature where the maximum in the C_p curve is located, the profile of $C_p(T) - C_{lattice}(T)$ across T_{OO} also changes as a function of the La doping. The integral of $C_p(T) - C_{lattice}(T)$ above T_{OO} increases with increasing of La doping x, as seen in Fig 7. This observation shows that La doping enhances critical fluctuations above T_{OO}.

For x = 0.50, an entropy change of 3.48 J/mol K at T_N is larger than the total entropy change at T_{OO} and T_N for YVO_3. This suggests that the transition for x = 0.50 may not be simply a magnetic ordering as happened at T_N for YVO_3. If we define T_N as the temperature where the maximum in the specific-heat curve is located, a larger amount of entropy is released above T_N for x = 0.50 compared with YVO_3 (see Fig 8). This observation signals that significant fluctuations associated with either orbital or spin persist above T_N for x = 0.50. Short-range spin correlations having a life time longer than the optical-mode lattice deformations that stabilize orbital ordering would introduce regions of strong spin-orbit coupling and/or competing orbital orders above T_N. This competition would inhibit long-range orbital order below T_N. The entropy change associated with the phase transition for x = 0.50 takes place over a wider temperature range (75 K $\leq$ T $\leq$ 180 K) compared with 90 K $\leq$ T $\leq$ 120 K for YVO_3. The T_N for YVO_3 determined from the C_p data is similar to that from the magnetic measurements; for x = 0.50, the T_N = 116 K from the C_p data is 6 K below the T_N = 122 K from magnetic measurement.

Figure 9 shows the effect of a magnetic field on the specific heat for x = 0.10. An applied magnetic field of 5 T does not shift T_{CG}, which means the relative stability of C-OO and G-OO phases is not affected. The lambda anomaly centered at T_{OO} shows no obvious change. At T_{OO}, the entropy change of 0.62 J/mol K under a 5 T magnetic field is marginally smaller than the 0.67 J/mol K obtained without magnetic field. On the other hand, the lambda anomaly centered at T_N broadens and is shifted a little to higher temperatures. This field effect has been observed in other perovskites where the spin ordered phase has weak canting.[13]

For $0.20 \leq x \leq 1$, the magnetic order at T_N is accompanied by a lattice anomaly. Figure 10 shows the lattice parameter change for x = 0.30 and 0.858, which serve as the example for Y-rich and La-rich region, respectively. The structure change starts at $T_t \approx T_N$. Our data do not resolve whether T_t is a few degree below T_N as in $LaVO_3$ and $CeVO_3$. Upon cooling across T_N, b-axes for x = 0.30 and x = 0.858 show opposite temperature dependence, which signals different magnetic/orbital ground states. This is confirmed by neutron powder diffraction measurements. Figure 11 shows the magnetic reflections for 5 different compositions measured at 12 K. The (100) magnetic reflection in Pbnm notation suggests C-type magnetic order for x = 0.90; while the (101) and (011) reflections confirm the G-type magnetic order for x = 0.30. For x = 0.624, the broad, weak peak at $d \approx 4.5$ Å and the hump at $d \approx 5.5$ Å suggest the competition and coexistence of C-type and G-type short range magnetic orders.

Discussion

Phase Diagram

The critical temperatures are summarized and plotted in the phase diagram of Fig. 1(b). In the interval $0 \le x \le 0.18$, the long-range magnetic order below $T_N < T_{OO}$ occurs within an orbtially ordered phase; for $0.20 \le x \le 1$, no long range orbital order is observed above T_N and the magnetic ordering at T_N is accompanied by a structural change at $T_t \le T_N$ as found for $CeVO_3$ and $LaVO_3$. Our neutron powder-diffraction study observed only G-SO diffraction reflections for x = 0.30 and only C-SO reflections for x = 0.90 in the temperature interval $10\ K \le T \le T_N$. In the intervals $0.20 \le x \le 0.40$ and $0.738 < x \le 1.0$, T_N increases with La doping; therefore, we assign G-SO for $0.20 \le x \le 0.40$ and C-SO for $0.738 \le x \le 1.0$. In the composition interval $0.40 < x < 0.738$, the large A-site variance broadens the diffraction peaks and lowers the neutron-diffraction peak intensities to where the detection of magnetic structure is difficult and time consuming. However, a composition independent T_N and weak features in neutron powder diffraction pattern for x = 0.624 suggest the coexistence of C-SO and G-SO magnetic clusters. With respect to the orbital ordering, we tentatively assume C-OO for $0.20 \le x \le 0.40$ and G-OO for $0.738 \le x < 1.0$ based on the evolution with temperature of the spin/orbital ordering in YVO_3 and $LaVO_3$.

Compared with Fig. 1(a), the following features in Fig. 1(b) are noteworthy:

(1) In the composition interval $0 \le x \le 0.18$ ($1.075 \le IR \le 1.10$ Å), T_{OO} and T_N decrease while T_{CG} increases with La doping. The IR dependence of these critical

temperatures is opposite to that in Fig. 1(a) in the same IR range. This IR dependence has been confirmed to be due to the A-site variance.[8]

(2) At $x \approx 0.20$ (IR ≈ 1.10 Å), the magnetic ordering temperature shows a sudden jump from 111 K for $x = 0.18$ to 116 K for $x = 0.20$. This sudden jump is accompanied by the disappearance of T_{OO} and T_{CG}.

(3) A characteristic temperature $T^* > T_N$ is defined by a deviation of $1/\chi(T)$ from a linear temperature dependence and an enhancement of $1/\kappa(T)$ where orbital order occurs only below T_N. The disordered state II in the interval $T_N < T < T^*$ appears to be characterized by a competition between G-OO, C-OO, and possible spin-orbit coupling. In Fig. 1(b), this competition is resolved below $T_t < T_N$ in favor of C-OO in the range $0.20 \leq x \leq 0.40$ and in favor of G-OO in the range $0.738 \leq x \leq 1.0$. In the interval $0.40 < x < 0.738$, the competition is manifest below T_N by an apparent phase separation. In Fig. 1(a), where the G-OO is stabilized below a $T_{OO} > T_N$, the G-OO/C-SO phase is stabilized to lowest temperatures for IR > 1.10 Å in single-crystal samples. The disordered state II only appears in Fig. 1(a) for R = Ce and La where orbital order sets in below T_N with an apparent first-order orbital flipping from C-OO to G-OO at a $T_t < T_N$. In Fig. 1(b), the G-SO below T_N is in sharp contrast to the C-SO of Fig. 1(a) in the range 1.10 < IR < 1.14 Å.

(4) The dashed curve in Fig. 1(b) denotes the existence of a lattice anomaly at $T_t \leq T_N$. A systematic structure study demonstrates that for $0.20 \leq x \leq 1$, a lattice change takes place at a $T_t \leq T_N$. An obvious lattice parameter change starts at T_N on cooling. However, the A-site variance decreases the magnitude of the lattice

change and broadens the transition. The dashed curve illustrates the existence of a lattice anomaly at T_t, but not the exact transition temperature.

Additional Suppression of κ(T)

An additional suppression of the glass-like thermal conductivity in the temperature interval $T_N \leq T \leq T^*$ for $0.20 \leq x \leq 1.0$ is in sharp contrast to the temperature dependence of κ(T) for $Y_{1-x}La_xVO_3$ ($0.0 \leq x \leq 0.18$) and for RVO_3 (R = Pr,…, Lu) where there is a well-defined $T_{OO} > T_N$. For the latter compositions, the temperature dependence of 1/κ(T) is characterized by slope changes at T_{OO} and T_N and a step-like jump at T_{CG} [9]. The glassy phonon thermal conductivity at $T > T_{OO}$ has been attributed to spin and orbital fluctuations. The phonon thermal conductivity is only partially recovered at $T_N < T < T_{OO}$ because of the retention of some orbital degree of freedom in the G-OO phase. At $T_{CG} \leq T \leq T_N$, the phonon thermal conductivity is further enhanced by the magnetic order and a possible magnon contribution, but it is not fully recovered; orbital and spin degrees of freedom still remain because of a competition between G-OO/C-SO and C-OO/G-SO phases. At $T = T_{CG}$, a step-like recovery of the phonon thermal conductivity characterizes the transition from the G-OO/C-SO state to the low temperature C-OO/G-SO state, which has little orbital or spin degree of freedom. Removal of orbital or spin fluctuations always enhances the phonon thermal conductivity. For $Y_{1-x}La_xVO_3$ ($0.20 \leq x \leq 1.0$), this enhancement has been illustrated by a recovery of thermal conductivity below T_N. The additional suppression of the glass-like phonon thermal conductivity in the

temperature interval $T_N \leq T \leq T^*$ signals, therefore, enhanced orbital fluctuations that can be due to competitions between G-OO, C-OO, and spin-orbit coupling.

For $Y_{1-x}La_xVO_3$ ($0.0 \leq x < 0.20$), the A-site variance introduced by partial replacement of Y by La lowers the stability of the G-OO phase, which enhances the relative stability of the C-OO phase below T_N. In the temperature interval $T_N < T < T^*$ of compositions $0.20 \leq x \leq 1.0$, short-range spin fluctuations may be slow enough below T* for cooperative orbital fluctuations arising from spin-orbit coupling $\lambda \mathbf{L} \bullet \mathbf{S}$ to compete with the G-OO and C-OO ordering, both of which suppress the orbital angular momentum. Competitive orbital ordering can be expected to introduce short-range fluctuations of orbitally ordered regions that suppress the thermal conductivity by phonons.

RVO_3 vs $RTiO_3$

RVO_3 ($3d^2$) and $RTiO_3$ ($3d^1$) perovskites are two important families to explore the orbital physics of t-electrons. Although intensive work has been carried out, the orbital-spin structure in $RTiO_3$ perovskites is still debated.[15,16] Here we restrict ourselves to the phase diagrams for RMO_3 and $Y_{1-x}La_xMO_3$ for M = Ti vs M = V.

The dramatic difference between Fig 1(a) and Fig 1(b) is in sharp contrast to the strong similarity between the phase diagrams for $RTiO_3$ and $Y_{1-x}La_xTiO_3$ (see Ref [15]). An important difference between the two systems is the degree of localization of the 3d

electrons. In the vanadate perovskites (both RVO_3 and $Y_{1-x}La_xVO_3$), they are definitely localized. In the titanate perovskites (both $RTiO_3$ and $Y_{1-x}La_xTiO_3$), they are strongly correlated, but the magnetism may be associated with narrow-band π^* electrons rather than localized t^1 configurations. The other major difference is a t^1 or π^{*1} manifold in titanate vs. a t^2 configuration in vanadate perovskites. This latter difference affects the way an intrinsic site distortion of orthorhombic perovskites biases the orbital ordering. An intrinsic site distortion accompanies the cooperative $MO_{6/2}$ octahedral-site rotations responsible for the orthorhombic distortion. Goodenough and Zhou[17] have shown that for an IR < 1.11 Å, the site distortion consists of long O-M-O bonds alternating with medium O-M-O bonds in the (001) planes (space group Pbnm); the *c*-axis bonds are shortest. As the IR > 1.11 Å increases, another component of the site distortion grows; it is a decrease of the site 90° O-M-O bond angle that subtends the rotation of *b* axis. With a t^2 configuration, the anitferroic component of the intrinsic site distortion, which is a maximum at IR ≈ 1.11 Å, biases the orbital ordering to be either G-OO or C-OO, an ordering that quenches the orbital angular momentum. Since this bias does not distinguish between G-OO and C-OO, other factors such as magnetic order or the other component of the site distortion can influence the competition between G-OO and C-OO. On the other hand, a t^1 configuration must respond to the component of the site distortion that opens up opposing faces of the octahedral sites. Therefore, an $\alpha < 90°$ O-M-O site distortion biases stabilization of the occupied orbital along a site [111] axis. This $(3z'^2-r^2)$ orbital, where $z' = [111]$, would then become half-filled, and a narrow half-filled band would couple nearest neighbors antiferromagnetically to give the G-SO found in antiferromagnetic $LaTiO_3$. On the other hand, with an $\alpha = 90°$ for an IR < 1.11 Å, the

($3z'^2 - r^2$) orbital is destabilized to leave a quarter-filled π^* band that gives rise to ferromagnetism in $YTiO_3$. In this case, the change in the orbital order produces an antiferromagnetic to ferromagnetic transition, and where the different orbital orderings are in competition, long-range magnetic order is suppressed. This competition gives a suppression of long-range magnetic order whereas the competition between G-OO and C-OO in the vanadate system has a more subtle effect on the magnetic order since each has anitferromagnetic coupling in the (001) planes, and a phase segregation can be accommodated without suppressing T_N.

Conclusions

We have plotted the phase diagram for spin and orbital ordering in $Y_{1-x}La_xVO_3$ ($0 \leq x \leq 1$). The extra stabilization of the C-OO phase by the introduction of an R^{3+}-ion variance causes the G-OO orbital-ordering temperature T_{OO} and C-SO magnetic ordering temperature T_N of YVO_3 to decrease and the first-order C-OO to G-OO orbital-flipping transition temperature T_{CG} to increase with increasing x until the long-range G-OO disappears and T_N intersects with T_{CG} at $x \approx 0.20$. Below T_N, the G-SO phase in the Y-rich region ($0.20 \leq x \leq 0.4$) is in contrast to the C-SO phase in the La-rich region ($0.738 \leq x \leq 1$). For $x \geq 0.20$, the variation of T_N with x is consistent with the coexistence of the two magnetically ordered phases for all temperatures $T < T_N$ in a compositional interval tentatively defined as $0.4 < x < 0.738$. The dramatic difference between Fig 1(a) and Fig 1(b) is in sharp contrast to the strong similarity between the phase diagrams for $RTiO_3$ and $Y_{1-x}La_xTiO_3$. This contrast can be traced to the different effect of the bias by the

intrinsic site distortions, which give rise to a different orbital/magnetic ordering competition in vanadate vs titanate perovskites.

*Present address: jqyan@utk.edu. Department of Materials Science and Engineering, University of Tennessee, Knoxville, Tennessee 37996. Materials Science and Technology Division, Oak Ridge National Laboratory, Oak Ridge, Tennessee 37831.

Acknowledgment

JQY thanks D. Khomskii for helpful discussion. JQY and RJM thank P. C. Canfield for enabling part of the magnetization measurements. JSZ, JGC, and JBG thank the NSF and the Robert A. Welch Foundation of Houston, TX, for financial support. This work was supported by the Division of Materials Sciences and Engineering, Office of Basic Energy Sciences, U.S. Department of Energy (U.S. DOE). Ames Laboratory is operated for the U.S. DOE by Iowa State University under Contract No. DE-AC02- 07CH11358. This work has benefited from the use of HIPD at the Lujan Center at Los Alamos Neutron Science Center, funded by DOE Office of Basic Energy Sciences. Los Alamos National Laboratory is operated by Los Alamos National Security LLC under DOE Contract DE-AC52-06NA25396. Use of the Advanced Photon Source was supported by the U. S. Department of Energy, Office of Science, Office of Basic Energy Sciences, under Contract No. W-31-109-Eng-38. Work at Argonne National Laboratory was supported by the U.S. Department of Energy, Division of Basic Energy Science-Materials Sciences, under Contract No. DE-AC02-CH11357 (the operation of IPNS).

Figure and Figure Captions

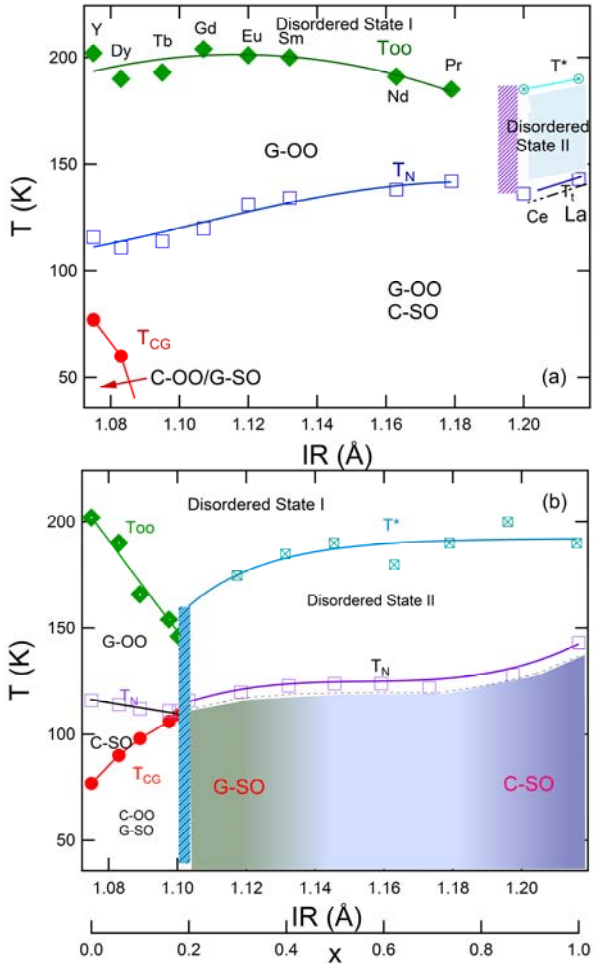

Fig. 1(color online) Spin and orbital ordering phase diagram for (a) RVO_3 (R = rare earth and Y) perovskites, and (b) $Y_{1-x}La_xVO_3$ ($0.0 \leq x \leq 1.0$). Transition temperatures in (a) are taken from Ref [1] and [9]. Transition temperatures in (b) are determined from magnetic measurements. Data for $x \leq 0.20$ in (b) are from Ref [8]. The rare earth radius in nine coordination is chosen since it is the highest coordination number available for all tabulated rare earths.[18] The solid curves are guides to the eye. The dashed curve below T_N denotes the existence of a lattice anomaly at $T_t \leq T_N$ for IR > 1.20 Å in (a) and 1.10 < IR ≤ 1.216 Å in (b).

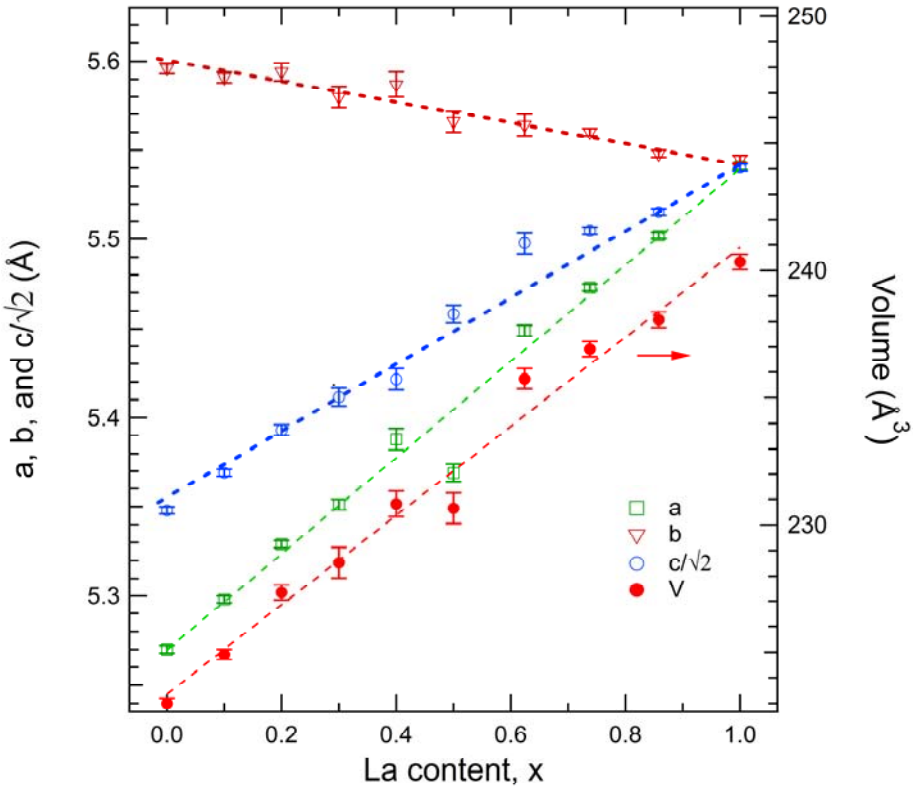

Fig. 2(color online) Room temperature lattice parameters determined with software Jade from X-ray powder diffraction patterns. The dashed lines are guide for eyes.

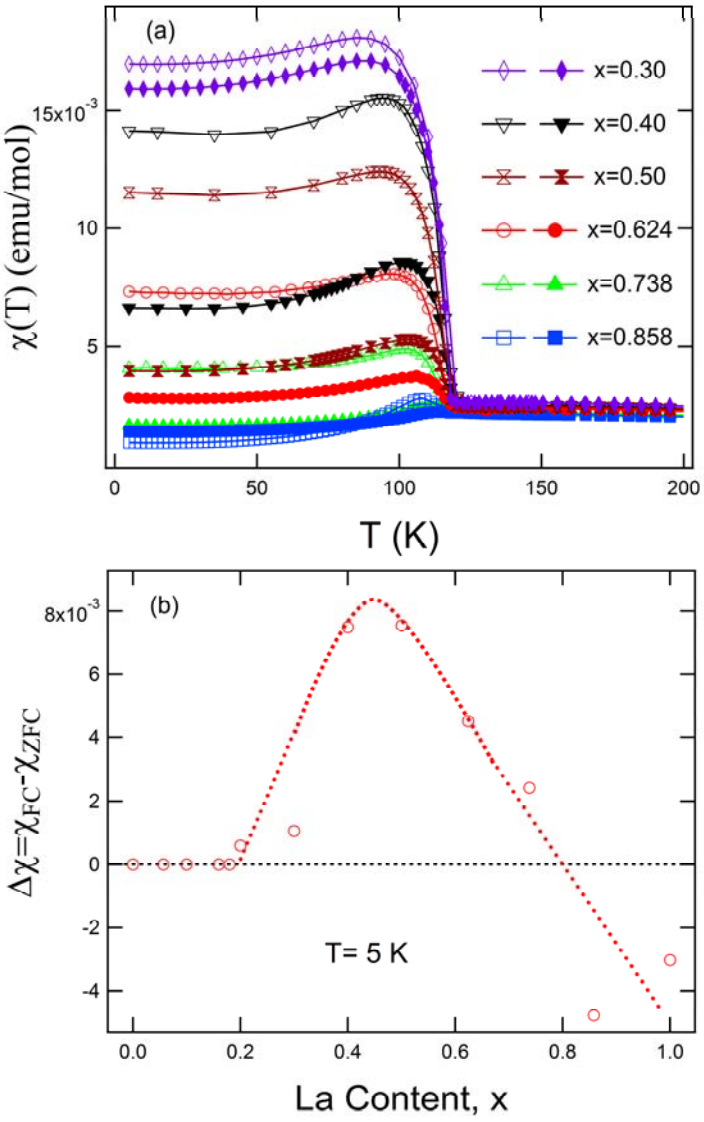

Fig. 3(color online) (a) Temperature dependence of magnetic susceptibility for $Y_{1-x}La_xVO_3$ ($0.30 \leq x \leq 0.858$) measured in FC (open) and ZFC (solid) modes in a field of 1 kOe. (b) Splitting between FC and ZFC curves for $Y_{1-x}La_xVO_3$ ($0.0 \leq x \leq 1.0$) at 5 K measured in a field of 1 kOe. The dashed curve is guide for eyes.

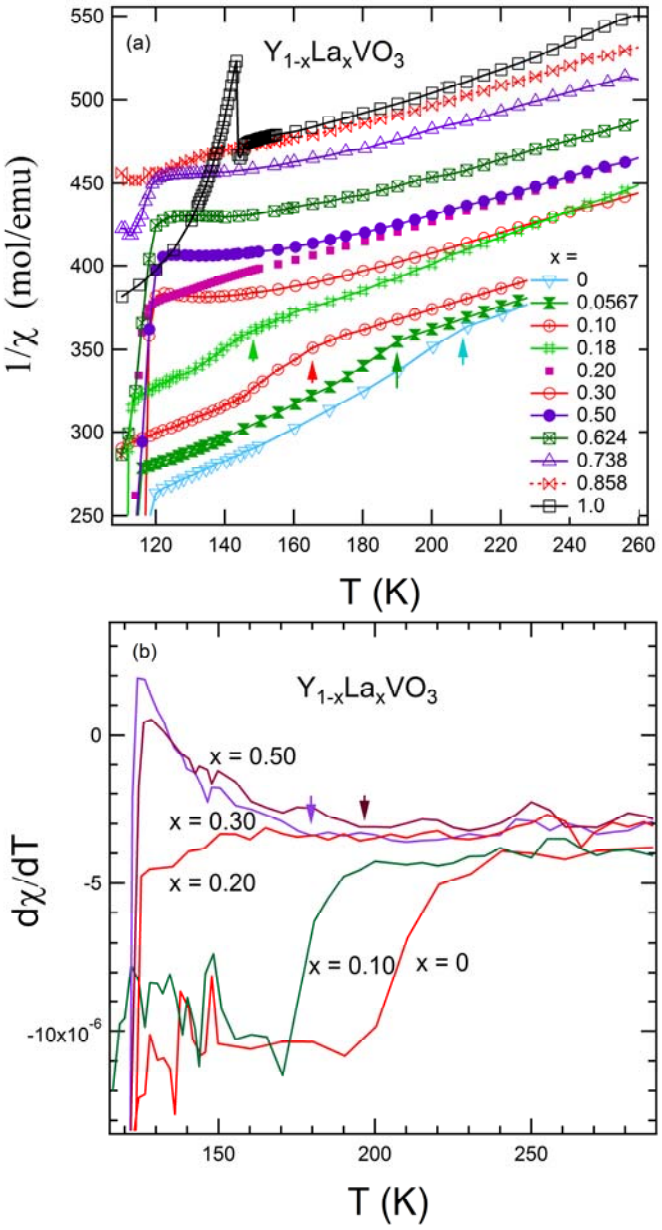

Fig. 4(color online) (a) Temperature dependence of reciprocal magnetic susceptibility for $Y_{1-x}La_xVO_3$ ($0.0 \leq x \leq 1.0$) measured in a ZFC mode in a field of 1 kOe. Solid arrows highlight the slope change at T_{oo}. (b) Derivative of magnetic susceptibility for $Y_{1-x}La_xVO_3$ ($0.0 \leq x \leq 0.50$) to highlight the different slope change at T_{oo} and T^*. Solid arrows show T^* for x = 0.30 and 0.50 determined from $d\chi/dT$.

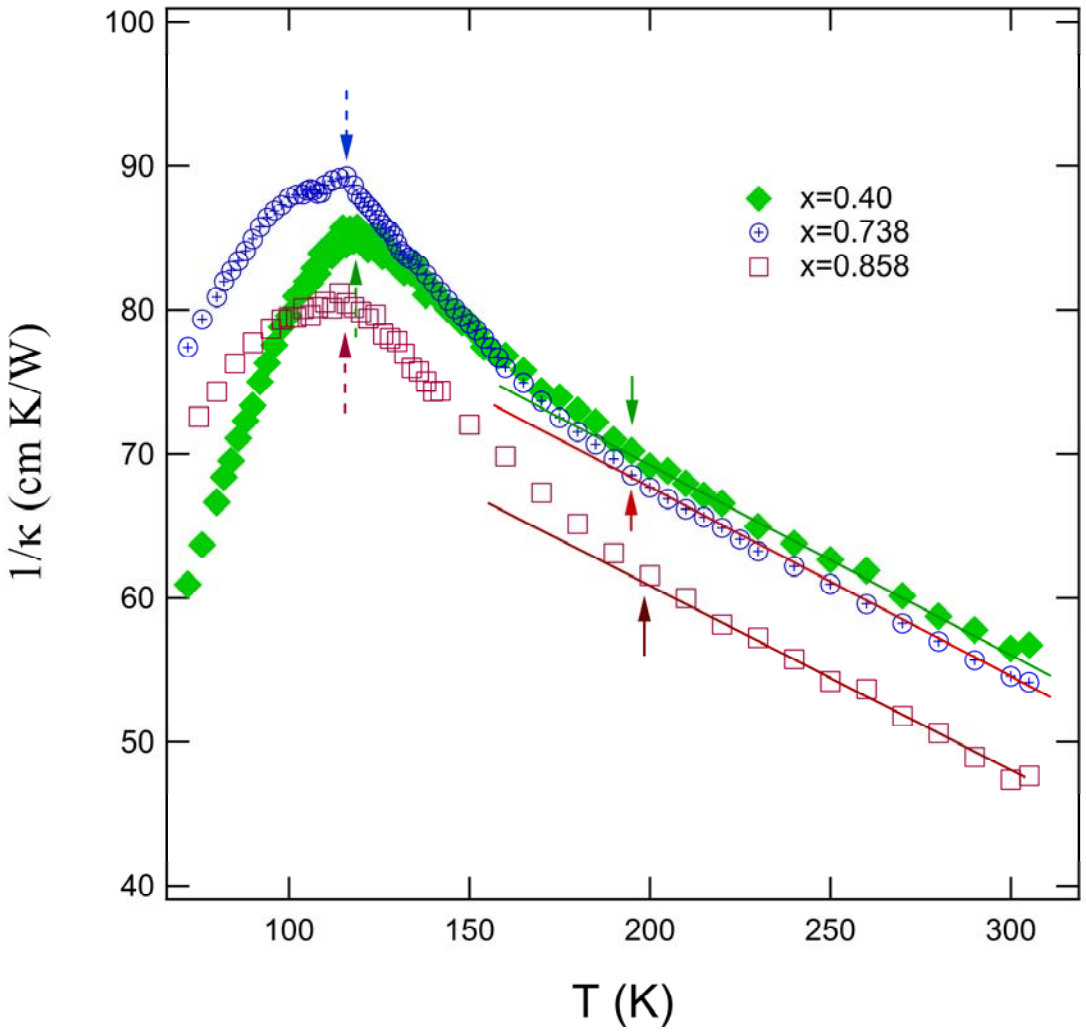

Fig. 5(color online) Temperature dependence of the reciprocal thermal conductivity for $Y_{1-x}La_xVO_3$ (x = 0.40, 0.738, and 0.858). The solid (dashed) arrows show T^* (T_N) determined from reciprocal thermal conductivity data. The solid lines highlight the additional suppression of glass-like thermal conductivity in the interval $T_N < T < T^*$.

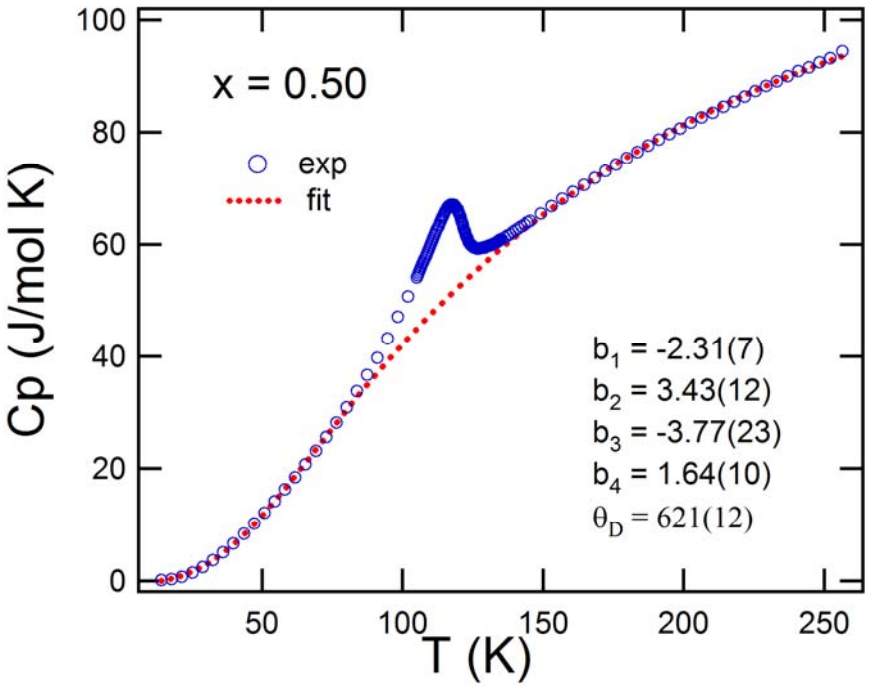

Fig. 6(color online) Temperature dependence of specific heat for $Y_{1-x}La_xVO_3$ (x = 0.50). The dashed curve shows the fit of lattice specific heat with Thirring model. The fitting parameters are also listed.

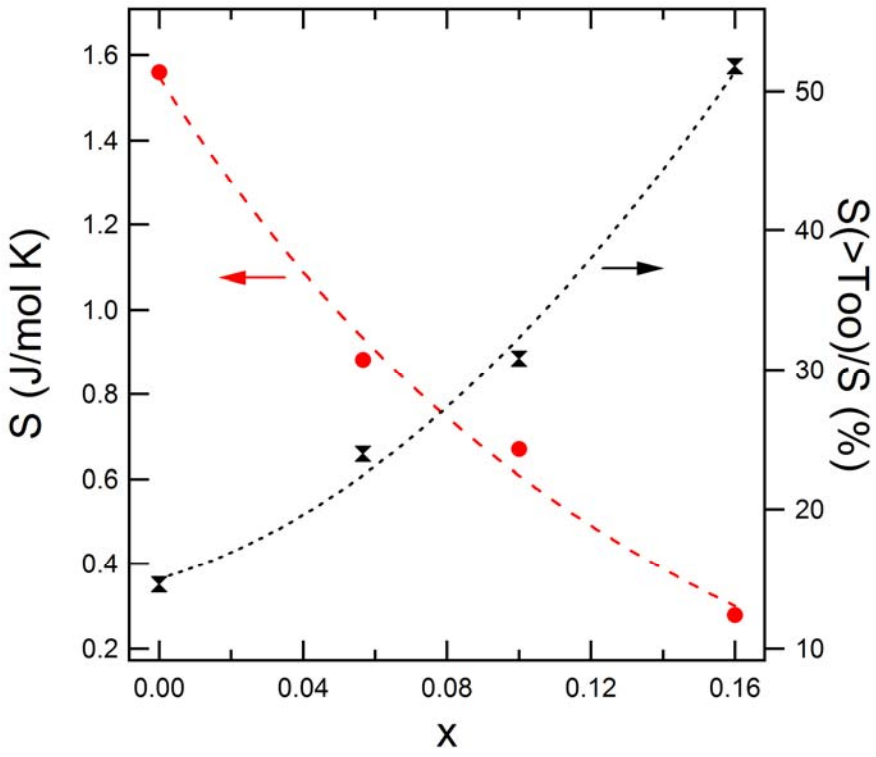

Fig. 7(color online) Doping dependence of the entropy change involved in the orbital ordering at T_{OO} for $Y_{1-x}La_xVO_3$ ($0.0 \leq x \leq 0.16$). The right axis shows the fraction of entropy change above T_{OO} as discussed in text.

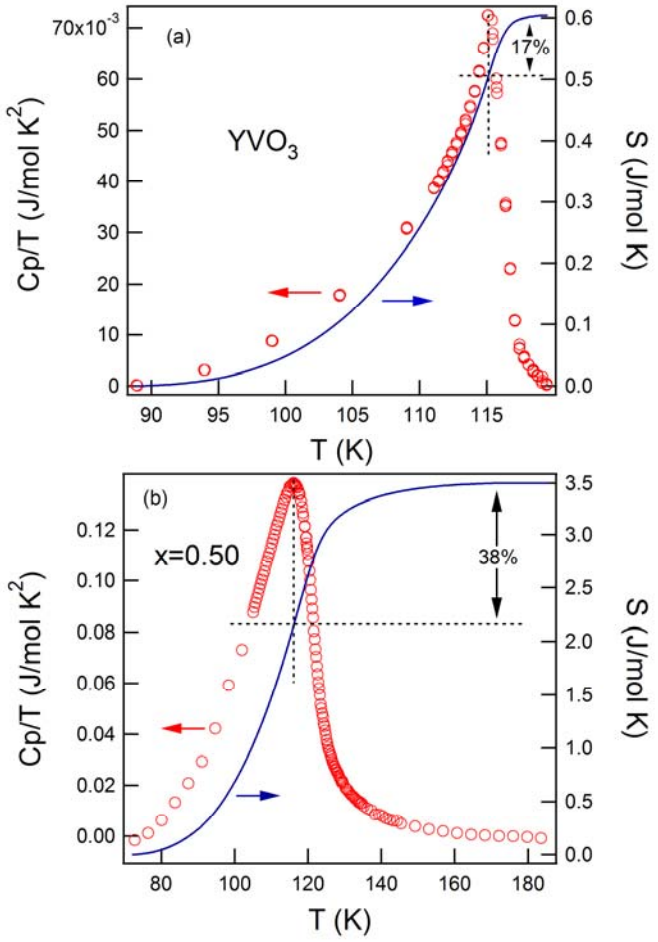

Fig. 8(color online) C_p/T versus T and the numerical integration of the entropy S after subtracting the lattice specific heat around T_N for YVO_3 and $Y_{0.50}La_{0.50}VO_3$.

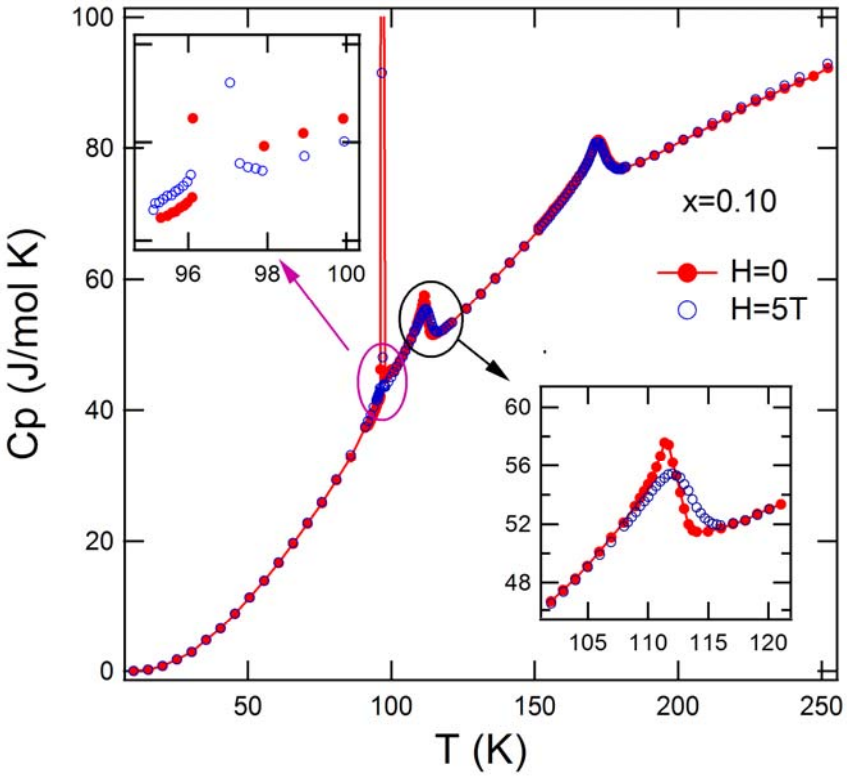

Fig. 9(color online) Magnetic field effect on the specific heat (C_p) of $Y_{1-x}La_xVO_3$ (x = 0.10). Zero field C_p data are from Ref [8].

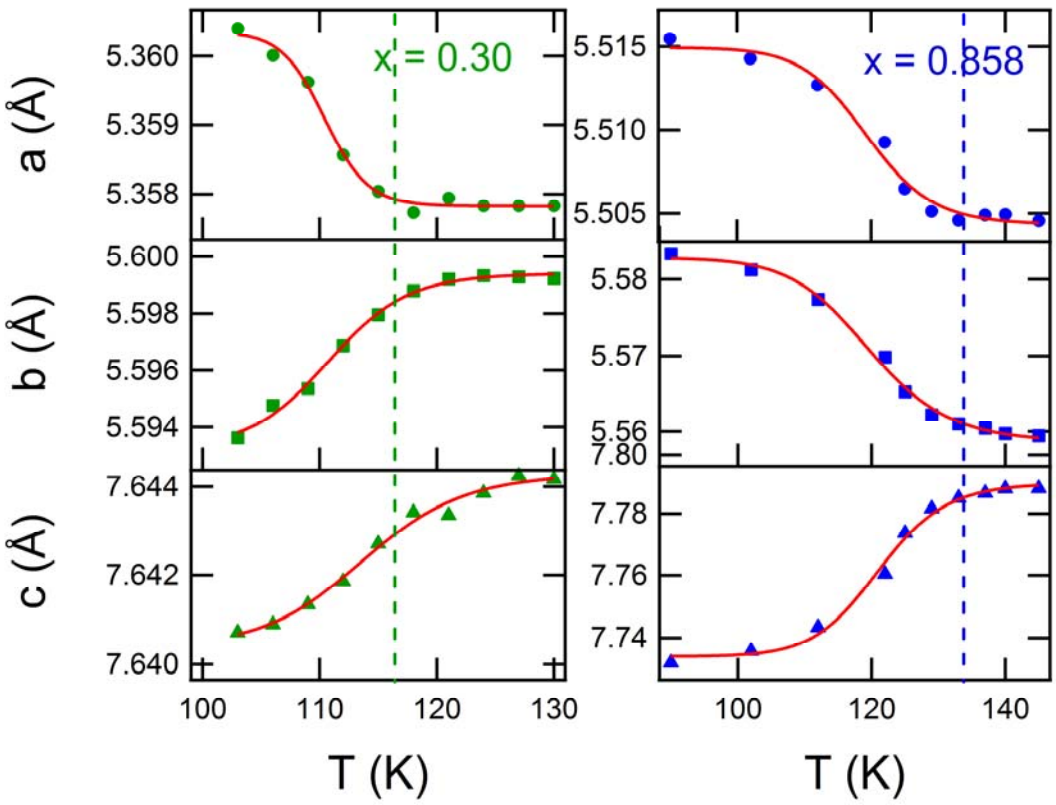

Fig. 10 (color online) Temperature dependence of lattice parameters for $Y_{1-x}La_xVO_3$ (x = 0.30 and 0.858) around T_N determined from synchrotron x-ray powder diffraction pattern. The solid curves are guide for eyes. The vertical dashed lines denote T_N.

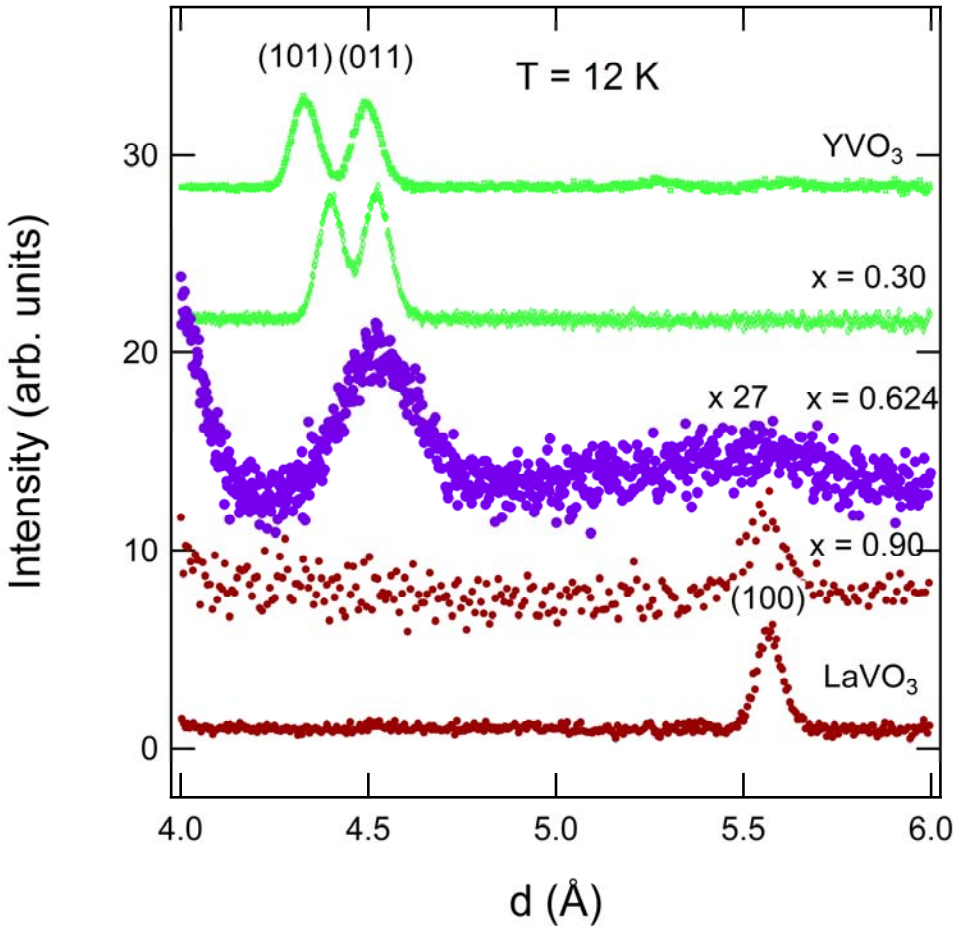

Fig. 11(color online) Magnetic reflections for $Y_{1-x}La_xVO_3$ ($0.0 \leq x \leq 1.0$) at 12 K. The curves were shifted for clarity. The intensity for x = 0.624 was scaled by a factor of 27 for clarity.

Reference

[1] S. Miyasaka, Y. Pkimoto, M. Iwama, and Y. Tokura, Phys. Rev. B **68**, R100406 (2003).

[2] G. R. Blake, T. T. M. Palstra, Y. Ren, A. A. Nugroho, and A. A. Menovsky, Phys. Rev. Lett. **87**, 245501 (2001).

[3] Y. Ren, A. A. Nugroho, A. A. Menovsky, J. Strempfer, U. Rutt, F. Iga, T. Takabatake, and C. W. Kimball, Phys. Rev. B **67**, 014107 (2003).

[4] A. Munoz, J. A. Alonso, M. T. Casais, M. J. Martinez-Lope, J. L. Martinez, and M. T. Fernandez-Diaz, Phys. Rev. B **68**, 144429 (2003).

[5] J.-S. Zhou, Y. Ren, J.-Q. Yan, J. F. Mitchell, and J. B. Goodenough, Phys. Rev. Lett. **100**, 046401 (2008).

[6] J. P. Attfield, A. L. Kharlanov, and J. A. McAllister, Nature (London) **394**, 157 (1998).

[7] H. C. Nguyen and J.B. Goodenough, Phys. Rev. B **52**, 324 (1995).

[8] J.-Q. Yan et al, Phys. Rev. Lett. **99**, 197201 (2007).

[9] J.-Q. Yan, J.-S. Zhou, and J. B. Goodenough, Phys. Rev. Lett. **93**, 235901 (2004).

[10] J.-Q. Yan, J.-S. Zhou, and J. B. Goodenough, Phys. Rev. B **72**, 094412 (2005).

[11] Y. Ren, et al., Phys. Rev. B **62**, 6577 (2000).

[12] H. Thirring, Z. Phys. **14**, 867 (1913).

[13] J. G. Cheng, et al., J. Phys.: Condens. Matter **17**, 5869 (2005).

[14] G. R. Blake, T. T. M. Palstra, Y. Ren, A. A. Nugroho, and A. A. Menovshy, Phys. Rev. B **65**, 174112 (2002).

[15] M. Mochizuki and M. Imada, New Journal of Physics **6**, 154 (2004). and references in

[16] I. V. Solovyev, Phys. Rev. B **74**, 054412 (2006).

[17] J.-S. Zhou and J. B. Goodenough, Phys. Rev. Lett. **94**, 065501 (2005).

[18] R. D. Shannon, Acta Cryst. A **32**, 751 (1976).